Project	**IEEE 802.16 Broadband Wireless Access Working Group <http://ieee802.org/16>**
Title	**Simulating Correlated Shadowing in Mobile Multihop Relay/Ad-hoc Networks**
Date Submitted	**2006-06-30**
Source(s)	Zhenyu Wang Eustace K. Tameh Andrew Nix University of Bristol Merchant Venturers Building Woodland Road, Bristol UK BS8 1UB Voice: +44 (0) 117 954 5169 Fax: +44 (0) 117 954 5206 [mailto: Zhenyu.Wang@bristol.ac.uk] [mailto: Tek.Tameh@bristol.ac.uk] [mailto: Andy.Nix@bristol.ac.uk]
Re:	This contribution is in the response of call for contribution issued for 802.16j project on July 3rd, 2006.
Abstract	This document investigates the joint spatial correlation property of the shadowing process for peer-to-peer radio links (mobile-to-mobile) in urban environments. A sum-of-sinusoids (SOS) based simulation model is proposed to generate the joint correlation shadowing process for system level simulations involving mobile multihop relay/ad-hoc networks.
Purpose	For approval and submission to IEEE 802.16j for system evaluation methodology
Notice	This document has been prepared to assist IEEE 802.16. It is offered as a basis for discussion and is not binding on the contributing individual(s) or organization(s). The material in this document is subject to change in form and content after further study. The contributor(s) reserve(s) the right to add, amend or withdraw material contained herein.
Release	The contributor grants a free, irrevocable license to the IEEE to incorporate material contained in this contribution, and any modifications thereof, in the creation of an IEEE Standards publication; to copyright in the IEEE's name any IEEE Standards publication even though it may include portions of this contribution; and at the IEEE's sole discretion to permit others to reproduce in whole or in part the resulting IEEE Standards publication. The contributor also acknowledges and accepts that this contribution may be made public by IEEE 802.16.
Patent Policy and Procedures	The contributor is familiar with the IEEE 802.16 Patent Policy and Procedures <http://ieee802.org/16/ipr/patents/policy.html>, including the statement "IEEE standards may include the known use of patent(s), including patent applications, provided the IEEE receives assurance from the patent holder or applicant with respect to patents essential for compliance with both mandatory and optional portions of the standard." Early disclosure to the Working Group of patent information that might be relevant to the standard is essential to reduce the possibility for delays in the development process and increase the likelihood that the draft publication will be approved for publication. Please notify the Chair <mailto:chair@wirelessman.org> as early as possible, in written or electronic form, if patented technology (or technology under patent application) might be incorporated into a draft standard being developed within the IEEE 802.16 Working Group. The Chair will disclose this notification via the IEEE 802.16 web site <http://ieee802.org/16/ipr/patents/notices>.

Simulating Correlated Shadowing in Mobile Multihop Relay/Ad-hoc Networks

Zhenyu Wang, Eustace K. Tameh, Andrew Nix
University of Bristol

I. Introduction

In a mobile multihop relay/ad-hoc network, mobiles tend to connect to each other and the basestation through a number of peer-to-peer (P2P) wireless links. One of the core ideas behind this is the provision of high capacity connectivity through P2P links. These short-range connections avoid large shadowing losses, and thus reduce transmit power and offer more efficient spatial reuse of the radio resource [1]-[6]. The need to evaluate the performance of routing protocols and radio resource management (RRM) schemes in such networks calls for channel models that properly reflect the cross spatial correlation properties of the shadowing process for mesh links between mobile nodes.

Most existing shadowing correlation models [7]-[11] are established based on the basestation (BS) to mobile station (MS) propagation channel for cellular networks, where only the MS moves. In [12], the cross-correlation of MS to multi-BS links was modelled for handoff performance analyses. The shadow fading between two BS and two MS was studied in [13]. However, in a multi-hop or ad-hoc network, the shadowing correlation property over a large numbers of MS-MS links (where the MS are free to move at both ends of the link) requires close investigation. In [14] it was reported that incomplete consideration of the spatial correlation in a multipoint-to-multipoint (M2M) radio channel (i.e. multiple MS-MS links) can lead to significant simulation inaccuracies, especially for routing protocol and RRM performance evaluation. In the first part of this submission we investigate the joint spatial correlation property of the shadowing process for meshed P2P/ad-hoc wireless links in a dense urban environment. This shadowing correlation for dual terminal mobility links is modelled using a joint correlation function (JCF). The analysis is based on channel data obtained from a detailed site specific three-dimensional ray tracing model. This model was previously developed and validated at the University of Bristol [16][17].

In addition to the correlation model discussed above, it is also necessary to develop an appropriate simulation model (presented in this document) to generate correlated shadowing for system level performance evaluation. In [13], a general mathematical joint correlation model with two BSs and two MSs was derived. In the 3GPP Spatial Channel Model (SCM) [15], it is suggested to introduce correlation between channels from one mobile to two base stations by multiplying random Gaussian variables with an appropriate correlation matrix. However, these approaches are impractical when applied to true P2P networks due to the large number of meshed channels between mobile nodes. In [15], the fast fading correlation between antenna elements in a MIMO channel was introduced by pre-generating a set of directional multipaths. Unfortunately, this method can not be used for generating correlated shadowing unless we know and are able to model the spatial correlation properties of the scatterers seen by all radio nodes in the test area, which is far from trivial. In [14] it is suggested to apply a simple biased fading (random or site-specific) process to each MS, however no detailed method is provided. We conclude that no efficient shadowing process models are currently available in the literature to support system level P2P and ad-hoc simulations.

In the second part of this submission, a sum of sinusoids (SOS) simulation model is proposed to generate the joint shadowing process in an urban P2P wireless network. The SOS method has been shown to have many advantages, particularly in terms of accuracy and speed for simulating fast fading channels [19]-[22]. One example of the method is the popular Jake's simulation model for Rayleigh fading channels [26]. Recently, the

SOS method has been used to simulate the one dimensional shadowing process for a BS-MS radio link [20], and the two dimensional shadowing process [11] that accommodates the situation where the MS moves along a closed route (i.e. a route with a common start and end point), rather than a straight line. In this submission, a discrete Monte Carlo sampling method (DMCM) is proposed to determine the spatial frequencies of the sinusoidal waveforms according to the spatial power spectrum, which is calculated from the JCF developed in the first part of this document. The performance of the resulting channel simulator is analyzed in terms of the average squared error (ASE) of the corresponding JCF relative to the theoretical (and hence desired) JCF, the shadowing Cumulative Distribution Function (CDF), and the simulation speed. Simulations are used to illustrate the potential of the newly proposed model.

The remainder of this document is organized as follows: In section II, the system model and assumptions are described. In section III, the 3D ray model used to obtain channel data is introduced, and the shadowing correlation property is analysed. The proposed simulation model is presented in section IV. An analysis of the proposed model is given in Section V together with a step by step implementation guide. A number of concluding remarks are drawn in Section VI.

II. System Model and Assumptions

Fig. 1 illustrates a physical model of an ad-hoc network with meshed P2P links. We denote a radio node in the network by $X_i := (x_i, y_i)$, with x_i and y_i representing the two physical location coordinates in a given test area. The radio nodes directly transmit to one another, with each node being capable of acting as a transmitter (Tx) or a receiver (Rx). The shadowing (shadow fading) fluctuation in radio link (i, j) is denoted by $s_{i,j}$, which is defined as the variance in the local path loss (averaged over tens of wavelengths) around the distance dependent mean path loss (averaged over a large number of Tx and Rx locations in the same radio environment and at a given separation distance) [8][24].

Assuming that the shadowing fluctuation is wide sense stationary, $s_{i,j}$ can be characterized by its first-and second-order statistics. From various experimental results, it has been shown [8][23][25] that the shadowing fluctuation can be characterized by a zero mean Normal distribution (in dB). Hence $s_{i,j}$ can be modelled as in equation (1), where $N(0, \sigma_s)$ represents the Normal distribution with zero mean (μ=0) and standard deviation σ_s. For a conventional cellular network, the spatial correlation of the shadowing fluctuation is characterized by an auto-correlation function (ACF) for a single basestation to mobile (BS-MS) link [7]-[11], and by a cross-correlation function (CCF) from the MS to multiple BSs [12][13].

For an ad-hoc network, we assume that all nodes have the same configuration (e.g. antenna type and height) and that they communicate to one another through a common channel. Hence, the shadowing fluctuation seen by the nodes at both ends of the radio link are identical, i.e. $s_{i,j} = s_{j,i}$. This is quite different compared to a conventional cellular network, where the radio link is established between different types of equipment, e.g. a BS at 15m above ground level height and a MS at 1.5m height. Interchanging the BS and MS locations would result in different shadowing fluctuations, i.e. $s_{i,j} \neq s_{j,i}$. Based on the above assumptions, the standard deviation of $s_{i,j}$ can be estimated using equation (2), where $E\{\cdot\}_{i,j}$ represents the expectation operator over all possible nodes pair X_i and X_j. The CCF between the shadowing fluctuation in the two links (e.g. $s_{1,3}$ and $s_{2,4}$ in Fig. 1) has the same form as the ACF for a single link when the nodes at both ends move (e.g. one end moves from X_1 to X_2, while the other moves from X_3 to X_4). To distinguish between the ACF and CCF used for cellular networks in previous literature, the correlation function of the shadowing fluctuation in an ad-hoc network is referred to here as a joint correlation function (JCF).

Finally, as in prior literature [7]-[13], we assume that the spatial correlation function of the shadowing fluctuation is only a function of the distance moved by the nodes (i.e. their position shifts). More specifically,

the correlation is said to be isotropic (i.e. the same in all directions). Hence the JCF (i.e. R_s) can be expressed as in equation (3), where d_T and d_R represent movements of the transmitter and receiver respectively.

$$s_{i,j}\ [dB] = N(0, \sigma_s) \quad (1)$$

$$\sigma_s{}^2 = E\{s_{i,j}{}^2\}_{i,j} = E\{s_{j,i}{}^2\}_{j,i} = E\{s_{i,j}{}^2\}_i = E\{s_{i,j}{}^2\}_j \quad (2)$$

$$R_s(d_T, d_R) = \frac{E\{s_{i,j} \cdot s_{i',j'}\}}{\sigma_s{}^2}; \quad d_T = |X_i - X_{i'}|, d_R = |X_j - X_{j'}| \quad (3)$$

III. Shadowing Correlation Property

In order to characterize the shadowing fluctuation correlation in a P2P network accurately, it is necessary to obtain channel data between all the meshed links in the network. It is extremely difficult (as well as impractical) to obtain sufficient channel data samples by means of measurement alone. To overcome this limitation, a fully 3D deterministic propagation model [16] has been used to generate the significant sets of propagation data required to statistically analyse the shadowing processes. The model uses geographic data (terrain, building, foliage and ground cover data) to predict power as well as time, frequency and spatial dispersion in the radio channel. The model was developed at the University of Bristol over a period from 1996-2004 and has been validated for cellular (and microcellular) applications, where the Tx is located above (and well below) the rooftop level at frequencies of 2GHz and 5GHz [16][17]. For the low Tx height validation studies (based on a 3m high Tx and 1.5m high Rx) in [17], the mean error in the predicted received power level (compared to measurement) was -2.5dB, with an RMS error of 6.8dB. This level of accuracy represents the state-of-the-art for ray optical models in an urban environment with low mounted antennas.

In our previous study of the P2P radio channel [23], we found that the shadowing fluctuation of P2P links can be well modelled as a Gaussian process (Normal distribution). In this section, we focus on the correlation properties of the shadowing process.

Ray Model Simulations

Simulations are based on an area of central Bristol. This urban environment is representative of a European city with typical three storey building heights. The average building height and road width for this region is 12m (including pitched roofs) and 20m respectively. Vertical dipole antennas were assumed at the Tx and Rx. 3D antenna field patterns were incorporated in the model and features such as polarization are included in the power and path loss predictions. The impact of the human body and the effects of moving objects (such as vehicles) were not included in the analysis. The simulations were performed at frequencies of 2.1GHz and 5.2GHz.

To study the spatial correlation of the channel in the case where only one end of a link moves, 6 routes were defined as shown in Fig. 2. The simulations were performed with a fixed Tx location, and with the Rx moving along each of the defined routes (this is referred to as a ‘single terminal mobility’ scenario, to differentiate it from the case where terminals at *both* ends of the radio link are mobile). As the spatial correlation is environment dependent, to obtain the average correlation function, the 6 routes were placed in different areas of the map, with a total length of 8km. The Tx/Rx were located at 1.5m above ground level (AGL) to simulate mobile radio terminals (MS units). To compare with the well known shadowing fluctuation correlation property in a cellular network, the Tx height was varied to simulate a WLAN Access Point (AP) at 5m AGL and a microcellular BS at 15m AGL.

To study the P2P joint correlation function (where terminals at both ends of the link are free to move), a pair of routes were defined for each simulation, with one route representing Tx movement and the other representing Rx movement (this is referred to as a 'dual terminal mobility' scenario). 4 route pairs have been defined in the city centre area, with a total length of 2km for the Tx and 2km for the Rx. The route pairs are shown in Fig. 3. The Tx and Rx terminals were set to a height of 1.5m AGL. In both simulation scenarios, channel data was generated with the Rx (and the Tx in the dual terminal mobility scenario) moving along the pre-set routes at 1m intervals. The shadowing fluctuation data was calculated by subtracting the predicted local path loss (where the effects of fast fading were removed using suitable averaging) from the distance dependent mean path loss found in our previous P2P radio channel study [23].

Spatial Autocorrelation Function

The spatial correlation property of shadowing fluctuation in a single link, where only one end is free to move, can be characterized by its auto-correlation function (ACF). From previous experiments in literatures [9][10], it has been found that the spatial ACF of the shadow fading process can be modeled using an exponential decay function, which is represented by equation (4):

$$R_1(d_R) = R_s(0, d_R) = e^{-\frac{|d_R|}{d_{cor}}\ln 2} \qquad (4)$$

where d_R represents the movement of the Rx, and d_{cor} represents the de-correlation distance. The value of d_{cor} dependents on the environment and corresponds to the distance at which the correlation drops to 0.5.

In this document, the ACF is estimated by feeding the channel data from our single terminal mobility scenario into equation (3), where the parameter d_T is set to zero (i.e. only the Rx moves around). Since we assume that the shadowing fluctuation seen in the downlink is identical to that in the uplink for a P2P channel, the ACF for a moving Tx and a fixed Rx (i.e. $d_T = 0$) will have the same form. The ACF has been calculated for each of the 6 routes described in Section III-B. This data has been averaged and is plotted in Fig. 4. It can be observed from the figure that the estimated ACF curves agree the exponential decay function very well. And for the city of Bristol, the best fit (Least Squares Fitting) de-correlation distance d_{cor} for MS-MS link was found to be about 20m (19.6m at 5GHz, 20.2m at 2GHz) with RMS errors less than 0.002.

Furthermore, it can be seen from Fig. 4 that the ACF for a wide range of link types (BS-MS, AP-MS and MS-MS) are similar, not withstanding the varying Tx heights and operating frequencies. This is reasonable since the shadowing fluctuation is actually a result of the birth and death of multipaths, which corresponds to the changing scatterers in the vicinity of the Tx and Rx. During the simulations, only the Rx, i.e. the MS, is allowed to move, and hence the shadowing fluctuations are mainly caused by the changing environment (i.e. buildings) surrounding the MS. This is especially true when the Tx/Rx separation distance is much greater than the correlation distance (20m in our studies). In such situations, a 20m movement at the BS will have little impact on the shadowing fluctuation observed at the MS. It should be noted that differences in the distance dependent mean path loss between different channel types have already been removed during the calculation of the shadowing fluctuation, and hence this is not seen in the correlation properties. Furthermore, the standard deviation of shadowing fluctuation (which is studied in [23]) does not have any impact on the resulting correlation value.

Joint Spatial Correlation Function

The spatial correlation property of shadowing fluctuation in a radio link where both ends are in motion (or between two different links) is characterized by the joint correlation function. The JCF is estimated by feeding the channel data from our dual terminal mobility scenario into equation (3). Fig. 5 shows the averaged spatial

JCF for the shadowing fluctuations, where the Tx and Rx movement offsets (d_T and d_R) are limited to 100 meters. For shifts beyond 100m, the correlation coefficient was found to lie between 0.1 and -0.1.

Fig. 6 shows two slice planes through Fig. 5, for $d_T = 0$ and $d_R = 0$ respectively, i.e. the functions $R_s\ (0,\ d_R)$ and $R_s\ (d_T,\ 0)$, which correspond to cases where only the Rx or Tx move. As expected, the two curves are very close to the exponential decay ACF extracted previously from the single terminal mobility simulations, with mean absolute errors of 0.045 and 0.048, and RMS errors of 0.052 and 0.054 for $R_s\ (0,\ d_R)$ and $R_s\ (d_T,\ 0)$ respectively (within the distance interval [*0m, 100m*]).

Fig 5(b) shows a contour graph of the JCF. It can be seen that when the correlation coefficient is greater than 0.2, the contour lines are approximate straight and lie at an angle of 45°. This indicates that the movements of the Tx and Rx have an independent and equal impact on the JCF value. Assuming that the shadowing fluctuation is only a result of changes in the local scatterers around the moving terminals, and also that the terminal movements are uncorrelated at both ends of the link, the JCF can be approximated by the product of the two ACF functions as shown in equation (5). Using this approximation the mean absolute error and the RMS error between $R_s\ (d_T,\ d_R)$ and $R_s\ (d_T,0) \cdot R_s\ (0,d_R)$ are just 0.028 and 0.037 respectively, for $d_T, d_R \leq 100$m).

$$R_s(d_T, d_R) = R_s(d_T, 0) \cdot R_s(0, d_R) = e^{-\frac{|d_T| + |d_R|}{d_{cor}} \ln 2} \qquad (5)$$

IV. Simulation Model

As mentioned previously, it is essential to accurately regenerate the joint shadow fading process in P2P wireless communications. In the past, several design methodologies were developed to simulate the fading channel. The vast majority of these methods can be classified into one of three categories:

1) The sum of sinusoids (SOS) method, which is based on the fact that a Gaussian random process can be expressed as an infinite sum of sinusoids with random phases and properly selected frequencies [18]. In practice, a finite number of sinusoids can be used to approximate the Gaussian process, and this is used to reduce complexity [19]. This method is frequently used to simulate correlated fast fading processes (e.g. [19][26]), and has been used recently to model shadowing processes [11][20].
2) The filter based method, where channel data is generated by means of low-pass filtering a zero-mean white Gaussian noise process (e.g. [27][28]). The underlying principle is that a stationary Gaussian process can be generated by passing a sequence of white Gaussian random deviates through a filter whose frequency response is the square root of the Gaussian process' power spectral density (PSD) [29, p. 403].
3) Channel design methods based on Markov processes. This method is often used (e.g. [31][32]) to model radio link properties, such as the *Signal-to-Noise Ratio* (SNR) and the *Bit Error Rate* (BER), instead of using physical propagation characteristics.

The SOS approach has been shown to have considerable advantages in terms of accuracy and speed [19]-[22]. The statistical properties of SOS-based channel simulation models are presented in [21]. A fast implementation scheme based on a look-up table is recommended in [22]. The SOS method is studied in some detail in [19], with four different techniques developed to compute the coefficients of the simulation model.

In this section, a SOS based simulation model is proposed for the joint shadowing processes seen in urban P2P radio channels. A discrete Monte-Carlo sampling method (DMCM) is used to determine the spatial frequencies of the sinusoidal waveforms based on the spatial power spectrum, which is calculated from the JCF of the P2P shadowing process.

SOS Simulation Model

The simulation model for a Gaussian random process $s(t)$ based on the SOS method described in [19] can be expressed as a 1D function in time:

$$\hat{s}(t) = \sum_{n=1}^{N} c_n \cos(2\pi f_n t + \theta_n) \quad (6)$$

where $\hat{s}(t)$ is the proximate version of *s(t)*, N represents the number of sinusoids. Strictly speaking, when N is finite, the stochastic process $\hat{s}(t)$ is non-Gaussian. Nevertheless, the CDF of $\hat{s}(t)$ will be close to a Gaussian process if N is sufficiently large, e.g. in the range 6 to 30 according to [19]. $\{\theta_n\}_{n=1}^{N}$ represent sets of uniformly distributed random phase variables in the range [0, 2π). $\{f_n\}_{n=1}^{N}$ and $\{c_n\}_{n=1}^{N}$ represent the frequencies set and the corresponding amplitude coefficients set respectively, which are determined such that the resulting $\hat{s}(t)$ has an identical (or as close as possible) power spectral density (PSD) as that of $s(t)$. The PSD of the Gaussian random process $s(t)$ can be calculated by performing the Fourier transform of the ACF of $s(t)$ [18].

As mentioned previously, the shadowing fluctuation can be modelled using a Gaussian random process as a function of the Tx and Rx locations. We use *s(x,y,u,v)* to represent the shadowing fluctuation, with [*x, y*] and [*u, v*] indicating the Tx and Rx positions in the test area respectively. *s(x, y, u, v)* can also be presented as a function of time, *s(t)*, in cases where the Tx and Rx are in motion. The movements of Rx and Tx are represented as $\mathbf{d}_T := [\Delta x, \Delta y]^T$ and $\mathbf{d}_R := [\Delta u, \Delta v]^T$ respectively (where $[\cdot]^T$ represents the transpose operation). We now extend equation (6) to a 4D spatial Gaussian process to simulate the spatially correlated shadowing process for a P2P radio channel:

$$\begin{aligned}\hat{s}(x,y,u,v) &= \sum_{n=1}^{N} c_n \cos\left(2\pi \mathbf{f}_n [x,y,u,v]^T + \theta_n\right) \\ &= \sum_{n=1}^{N} c_n \cos\left[2\pi\left(f_{x,n}\, x + f_{y,n}\, y + f_{u,n}\, u + f_{v,n}\, v\right) + \theta_n\right]\end{aligned} \quad (7)$$

where $\hat{s}(x,y,u,v)$ determines the shadowing fluctuation value on a virtual map characterized by the spatial frequencies set $\{\mathbf{f}_n\}$, the corresponding coefficients $\{c_n\}$ and the phases $\{\theta_n\}$. The discrete spatial frequencies $\mathbf{f}_n := [f_{x,n}, f_{y,n}, f_{u,n}, f_{v,n}]$ represent four element vectors. We further define spatial frequencies $\mathbf{f}_{T,n} := [f_{x,n}, f_{y,n}]$, $\mathbf{f}_{R,n} := [f_{u,n}, f_{v,n}]$, and continuous frequency variables $\mathbf{f}_T := [f_x, f_y]$, $\mathbf{f}_R := [f_u, f_v]$ and $\mathbf{f} := [f_x, f_y, f_u, f_v]$, for the convenience of subsequent referrals.

We extend the ACF in equation (4) to a 2D function as expressed in equation (8) (for the case where just the Tx moves, which is similar to the case where just the Rx moves), and the JCF in equation (5) to a 4D function as expressed in equation (9).

$$R_1(\mathbf{d}_T) = e^{-\frac{|\mathbf{d}_T|}{d_{cor}}\ln 2} = e^{-\frac{\sqrt{\Delta x^2 + \Delta y^2}}{d_{cor}}\ln 2} \quad (8)$$

$$R_2(\mathbf{d}_T, \mathbf{d}_R) = R_1(\mathbf{d}_T) \cdot R_1(\mathbf{d}_T) \quad (9)$$

The spatial frequency set $\{\mathbf{f}_n\}$ and the coefficients $\{c_n\}$ for $\hat{s}(x,y,u,v)$ in equation (7) can be determined by sampling the 4D PSD of the Gaussian random process $s(x,y,u,v)$. To obtain the desired PSD, we need to perform the Fourier transform on the 4D ACF (i.e. the JCF, as explained in section II) of $s(x,y,u,v)$ in equation (9). This gives:

$$\Phi_2(\mathbf{f}) = \int_{-\infty}^{\infty}\int_{-\infty}^{\infty} R_2(\mathbf{d}_T,\mathbf{d}_R)\cdot e^{-j(2\pi\mathbf{f}_T\cdot\mathbf{d}_T+2\pi\mathbf{f}_R\cdot\mathbf{d}_R)}d(\mathbf{d}_T)d(\mathbf{d}_R)$$

$$= \int_{-\infty}^{\infty} R_1(\mathbf{d}_T)\cdot e^{-j\cdot 2\pi\mathbf{f}_T\cdot\mathbf{d}_T}d(\mathbf{d}_T)\int_{-\infty}^{\infty} R_1(\mathbf{d}_R)\cdot e^{-j\cdot 2\pi\mathbf{f}_R\cdot\mathbf{d}_R}d(\mathbf{d}_R)$$

$$= \Phi_1(\mathbf{f}_T)\cdot\Phi_1(\mathbf{f}_R) \qquad (10)$$

where $\Phi_2(\mathbf{f})$ represent the 4D PSD of $s(x,y,u,v)$, and $\Phi_1(\mathbf{f}.)$ is the Fourier transforms of the correlation functions $R_1(\mathbf{d})$ in equation (8). Equation (11) gives the closed-form solution of $\Phi_1(\mathbf{f}_T)$ (and a similar process gives $\Phi_1(\mathbf{f}_R)$), as derived in [11].

$$\Phi_1(\mathbf{f}_T) = \frac{2\pi a}{\left[a^2+4\pi^2|\mathbf{f}_T|^2\right]^{\frac{3}{2}}} = \frac{2\pi a}{\left[a^2+4\pi^2\left(f_x^{\,2}+f_y^{\,2}\right)\right]^{\frac{3}{2}}}, \quad a=\ln(2)/d_{cor} \qquad (11)$$

There are four methods proposed in [19] to sample the desired PSD in order to determine the spatial frequency set $\{\mathbf{f}_n\}$ and the coefficients $\{c_n\}$ in a SOS model. These methods have been used previously to model shadowing processes in [11] and [20]. They are:

1) The uniform sampling method (USM, also known as Equal Distance method),
2) The non-uniform sampling method (NUSM, also known as Equal Areas method),
3) The Monte Carlo Method (MCM), and
4) The Mean Squared Error Method (MSEM). (In [20], the author uses a general form, L_P-Norm Method (LPNM), with p = 2).

From the first three methods, it is found in [11] that the MCM, with the frequency set $\{\mathbf{f}_n\}$ generated according to a given *Probability Density Function* (PDF) (which in turn is determined by the PSD), gives the best performance in terms of average square error (ASE) of correlation functions of simulated shadowing process (the mathematic definition can be found in Section IV-C) versus the number of sinusoids N. However, this method has the highest computational complexity. The USM method, where the PSD is uniformly sampled with frequency spacing Δf, and $C_n^{\,2}/2$ represents the power of the PSD in the frequency interval $[f_n-\Delta f/2, f_n-\Delta f/2)$, requires a large number of sinusoids, but has two useful features:

i) The result $\hat{s}(\cdot)$ is a periodical function, which is desirable when the user wants to wrap the shadowing fluctuation values around the simulated radio environment to avoid interference edge effects, and/or to simulate a large network.

ii) It can be implemented using a look-up table on a computer or in hardware (which is fast).

It will be shown later in the analyses of the models that a large number of sinusoids are required to reduce the ASE of a 4D JCF, even when the MCM method is used; hence a high-speed simulation scheme is necessary. In the remainder of this section, we first describe the proposed Discrete Monte-Carlo Method (DMCM), which is a combination of MCM and USM. Following this, a number of performance evaluations are discussed. The MSEM presented in [19] and [20] does not have a closed-form solution, and is therefore not considered in this document.

Discrete Monte Carlo Method

In a pure MCM, the 4D spatial frequencies set $\{\mathbf{f}_n\}$ in equation (7) can be generated according to a given joint PDF, which is related to the PSD of the joint shadowing process. More specifically, the sampling frequencies

can be generated according to a PDF proportional to the PSD [32]. From equation (8), it is straightforward to decompose the joint PDF for $\mathbf{f}$ into two independent identical PDFs for $\mathbf{f}_T$ and $\mathbf{f}_R$, as shown in equation (12). Therefore, $\mathbf{f}_{T,n}$ and $\mathbf{f}_{R,n}$ can be generated independently:

$$p_2(\mathbf{f}) = b_2\Phi_2(\mathbf{f}) = b_2\Phi_1(\mathbf{f}_T)\Phi_1(\mathbf{f}_R) = b_1 p_1(\mathbf{f}_T)p_1(\mathbf{f}_R) \quad (12)$$

where $p_1(\cdot)$ and $p_2(\cdot)$ denote the 2D PDF and 4D joint PDF respectively, and b_1 and b_2 are constants that ensure the integration of the PDF equals unity. $p_1(\cdot)$ and the functions used to generate $\mathbf{f}_{T,n}$ (and $\mathbf{f}_{R,n}$, since it has an identical PDF) have been derived in [11]:

$$|\mathbf{f}_T| = \frac{a}{2\pi}\sqrt{\frac{1}{(1-\beta)^2}-1},\ f_x = |\mathbf{f}_T|\cos(\varphi),\ f_y = |\mathbf{f}_T|\sin(\varphi) \quad (13)$$

$$\theta_n = U(0,2\pi) \quad (14)$$

where β is a random variable uniformly distributed over the range [0,1], and φ is uniformly distributed over [0,2π). θ_n in equation (7) is a random variable uniformly distributed over [0, 2π), and can be expressed using (14). The coefficients $\{c_n\}$ have the same value for all sinusoids [19], and are defined by the total power of the Gaussian random process s.

To enable an efficient implementation of the MCM, we introduce an equivalent discrete realization of equation (7), named the Discrete MCM (DMCM). First, we define the frequency sampling interval to be $2\Delta f$, as in the USM method. We then modify the original sinusoid $\mathbf{f}_n$ from the pure MCM according to equation (16).

$$\bar{f}_{x,n} = round\left[\frac{f_{x,n}+\Delta f}{2\Delta f}\right]\cdot 2\Delta f - \Delta f = (2m_{x,n}+1)\Delta f \quad (15)$$

Where $m_{x,n}$ is an integer. $\bar{f}_{y,n}$, $\bar{f}_{u,n}$ and $\bar{f}_{v,n}$ are modified in the manner previously described by equation (15). This modification forces the resulting Gaussian random process to have a period $1/\Delta f$. We next set $\Delta\theta = 2\pi/N_{Table}$ to represent the resolution of the stored sinusoidal waveform, with table size denoted by N_{Table}. We now modify $\{\theta_n\}$ as:

$$\bar{\theta}_n = round\left(\frac{\theta_n - \Delta\theta/2}{\Delta\theta}\right)\times\Delta\theta = l_n\Delta\theta \quad (16)$$

where $l_n \in \{0,1,\ldots,N_{Table}-1\}$. Finally, we set the spatial sampling interval $\Delta x = 1/(N_{Table}\cdot\Delta f)$ and $[\bar{x},\bar{y},\bar{u},\bar{v}] = [k_x, k_y, k_u, k_v]\cdot\Delta x$, $k_\cdot \in \mathbb{Z}$. Equation (7) can now be rewritten in the discrete form shown below:

$$\bar{s}(\bar{x},\bar{y},\bar{u},\bar{v}) = \sqrt{\frac{N}{2}}\sum_{n=1}^{N}\cos\left\{\frac{2\pi}{N_{Table}}\left[(2m_{x,n}+1)k_x + (2m_{y,n}+1)k_y + (2m_{u,n}+1)k_u + (2m_{v,n}+1)k_v + l_n\right]\right\} \quad (17)$$

where $\bar{s}(\bar{x},\bar{y},\bar{u},\bar{v})$ represents a discrete Gaussian random process. It is easy to see from equation (17) that with $N_{Table}\to\infty$, the DMCM becomes a pure MCM when $\Delta f\to\infty$, or a pure USM when $N\to\infty$. As all the elements in the operator $\sum$ are in the set $\{cos(2\pi\cdot i/N_{Table}\cdot),\ i\in\{0,1,\ldots,N_{Table}-1\}$, equation (17) can be implemented on a computer using a look-up table, with all operations involving integers; hence simulation speed can be high. According to [22], equation (17) can be realized in a multiplier-free hardware simulator; however this falls outside the scope of this document.

In real P2P networks, all nodes normally communicate to one another through a common channel, and hence the shadowing fluctuation in the uplink and downlink is expected to be identical, i.e. $s(x,y,u,v) = s(u,v,x,y)$. In

order to account for this fact, we introduce the symmetric DMCM. Letting N be even, we first generate the first half of the frequency set $\{\mathbf{f}_n\}$, n=1,2,...,N/2, as described above. The second half of this set is then generated using:

$$\mathbf{f}_{n+N/2} = \mathbf{f}_n \cdot \begin{bmatrix} 0 & \mathbf{I} \\ \mathbf{I} & 0 \end{bmatrix}; \quad \mathbf{I} = \begin{bmatrix} 1 & 0 \\ 0 & 1 \end{bmatrix}, n = 1,2,...,N/2 \tag{18}$$

$$\theta_{n+N/2} = \theta_n, n = 1,2,...,N/2 \tag{19}$$

i.e. $\mathbf{f}_{T,n} = \mathbf{f}_{R,n+N/2}$ and $\mathbf{f}_{R,n} = \mathbf{f}_{T,n+N/2,}$ where n=1,2,...,N/2. It should be noted that $\mathbf{f}_{T,n}$ and $\mathbf{f}_{R,n}$ are still independently generated. The above modification makes the discrete spatial frequency set $\{\mathbf{f}_n\}$ symmetric with respect to (w.r.t.) $\mathbf{f}_T$=$\mathbf{f}_R$, which results in symmetric shadowing fluctuation values for the up and down links. This does not change the shape of the 4D joint PDF, since the PDF is symmetric in the same manner (i.e. w.r.t. $\mathbf{f}_T$=$\mathbf{f}_R$). We also let $\theta_n = \theta_{n+N/2}$, n=1,2,…,N/2. This modification prevents the phase set $\{\theta_n\}$ from containing purely random values, and thus introduces additional and unwanted correlations between $\mathbf{f}_n$ and $\mathbf{f}_{n+N/2}$. Therefore, some degree of degradation is expected for the DMCM when symmetric properties (symmetric DMCM) are required (compared to a non-symmetric DMCM). This degradation is analyzed in section V.

Performance Metrics

We propose three performance metrics to evaluate the Gaussian random process simulator: 1) the CDF of the output values of shadowing fluctuation, 2) the simulation speed, and 3) the ASE of the resulting correlation function.

The ASE of the correlation function was introduced in [11], and defined as the average squared error between the correlation functions of the simulated process $\hat{s}(\cdot)$ and the desired correlation functions of the shadowing process. It is equal to the square of the root mean square error (RMSE).

For the USM, MCM and the non-symmetric DMCM, given that the only random variables in (7) are $\{\theta_n\}$, the JCF (i.e. the 4D spatial ACF) of $\hat{s}(x,y,u,v)$ can be evaluated using equation (20), where $(\cdot)^*$ denotes complex conjugate.

$$\begin{aligned} R_{\hat{s}}(\Delta x, \Delta y, \Delta u, \Delta v) &= E\left\{\hat{s}(x,y,u,v)\hat{s}(x+\Delta x, y+\Delta y, u+\Delta u, v+\Delta v)^*\right\} \\ &= \sum_{n=1}^{N} \frac{c_n^{\,2}}{2} \cos\left[2\pi\left(f_{x,n}\Delta x + f_{y,n}\Delta y + f_{u,n}\Delta u + f_{v,n}\Delta v\right)\right] \end{aligned} \tag{20}$$

For the symmetric DMCM, equation (20) is no longer valid and $R_{\hat{s}}(\cdot)$ must be directly evaluated from the generated data.

The ASE of the JCF (*ASE*) can be evaluated using equation (21) via numerical integration. Since the Gaussian random process generated using the USM and symmetric DMCM is periodic, only the ASE between [*-1/(4Δf), 1/(4Δf)*] has to be evaluated for those methods. We let *X=Y=U=V=1/(2Δf)* since the JCF are symmetric with respect to *X=Y* (*U=V*).

$$\begin{aligned} ASE = \frac{1}{XYUV} &\int_{-X/2}^{X/2}\int_{-Y/2}^{Y/2}\int_{-U/2}^{U/2}\int_{-V/2}^{V/2} \\ &\left[R_{\hat{s}}(\Delta x, \Delta y, \Delta u, \Delta v) - R_2(\Delta x, \Delta y, \Delta u, \Delta v)\right]^2 d\Delta x\, d\Delta y d\Delta u\, d\Delta v \end{aligned} \tag{21}$$

V. Model Implementation and Numerical Results

In the following section we present a range of numerical results using the DMCM channel simulation model. The performance of the proposed model with different parameter settings is studied and compared against the pure MCM and USM in terms of the ASE of the JCF, the CDF of the output values, and the simulation speed. A step-by-step implementation guide is also given, together with suggestions on the parameter settings.

Numerical Results

The proposed model can be used to generate a virtual shadowing map with desired correlation properties. As the SOS method gives deterministic output, the virtual map is stored in terms of a set of sinusoids at each considered point, instead of the actual shadowing fluctuation values. The shadowing fluctuation for any Tx-Rx link within this virtual map is then calculated on demand. This enables the model to implement the shadowing process over a large geographic region without the need for excessive memory space. A step-by-step implementation guide for the proposed model can be found in section V-C.

Fig. 7 shows a realization of the SOS model using the symmetric DMCM. The de-correlation distance is set to 20m (from Section III-A), the number of discrete 4D spatial sinusoids N=500, and the lowest frequency Δf=1/500m. Hence the period of the output shadowing process is 500m. The sinusoid waveform table size is set to 200. As the discrete frequencies set $\{\bar{\mathbf{f}}_n\}$ are symmetric with respect to $\mathbf{f}_T$=$\mathbf{f}_R$, only $\bar{\mathbf{f}}_{T,n}$ are plotted in the figure. The output sample is generated by defining a number of Tx positions over a 500m x 500m grid with 2m spacings and fixing the Rx to lie at a location in the centre of the test area (single terminal mobility study). The 2D ACF is evaluated using the data from the single terminal mobility studies and plotted in Fig. 8, together with the theoretical ACF. To evaluate the JCF, the shadowing fluctuation data is generated from a route analysis, where both the Tx and the Rx move along two straight paths (dual terminal mobility study). The start points and the direction of motion for the Tx and Rx are random and independent. Fig. 9 shows the evaluated JCF, which is averaged over 10 dual terminal mobility studies on one arbitrary DMCM realization.

Performance Analyses

Fig. 10 illustrates the ASE level for the JCF. Without loss of generality, the spatial scale is normalized by the decorrelation distance, i.e. d_{cor}=1. We vary the number of spatial sinusoids N in the range 100 to 2000, Δf from 1/6 to 1/40*,* and the table size N_{Table} from 200 to 1000. For the symmetric DMCM, $R_{\hat{s}}(\cdot)$ is evaluated directly from the generated data in single/dual terminal mobility studies . The resultant ASEs are averaged over 30 realizations for each method.

It can be seen from Figs 10 that the USM has a better ASE performance compared to the other methods when Δf is less than 1/15. However, this performance is gained at the cost of an increased number of sinusoids as Δf decreases. E.g. for Δf=1/20 and a *30dB* cut-off frequency f_c =1.1 period/m (at which the amplitude of the PSD in equation (11) is 30dB lower than the amplitude at zero frequency), the number of sinusoids is $22^4/2$ for the 4D process using USM; with the number of sinusoids N=2048 (i.e. Δf=1/6), the ASE of USM is only 0.02, which is far poorer than other methods. The MCM offers the best performance compared to the symmetric and non-symmetric DMCM with the same number of sinusoids N. The ASE improves from 10^{-2} to 10^{-3} as the number of sinusoids is increased from 100 to 500 for both the 2D ACF and JCF.

The ASE performance of the non-symmetric DMCM is bounded by both the MCM and the USM performance. This is expected since the DMCM is a combination of these schemes. When Δf is greater than 1/10, the ASE level is high and little performance gain is achieved by increasing the number of sinusoids N. This indicates that the performance degradation is mainly due to the large frequency sampling interval. As Δf increases, the ASE level of the DMCM drops and finally reaches the ASE level of the MCM with the same number of sinusoids. For N less than 500, a non-symmetric DMCM can achieve a similar performance to the MCM when Δf reduces

to 1/20; while for N greater than 500, a smaller Δf value is required. The reduction of table size N_{Table} from 1000 to 200 is seen to have little effect on the ASE level. However, in a real implementation of the shadowing model, the table size should not be too small since it is inversely proportional to the spatial sampling interval Δx, which itself must be much less than de-correlation distance, i.e. the shadowing fluctuations at two adjacent sampling positions are highly correlated..

Compared to the non-symmetric DMCM, for the same parameter settings, the symmetric DMCM is seen to generate a higher ASE. To force symmetry, additional constraints were imposed on the phase of the sinusoids (see section IV-B). This introduces additional correlation between frequency sets $\bar{\mathbf{f}}_n$ and $\bar{\mathbf{f}}_{n+N/2}$, and thus a higher observed ASE. However, it can be seen from Fig. 10 that the degradation in performance can be reduced by increasing the frequency resolution $1/\Delta f$. For example, with the number of sinusoids N =100, the ASE level of the symmetric DMCM becomes very close to that of the non-symmetric DMCM when Δf decreases to less than 1/30.

Fig. 12 presents the CDF of the output values from the MCM and DMCM, both evaluated using 10^4 output samples from a single arbitrary realization for each method with random Tx and Rx positions. The results show that N =200 is adequate to approximate a Gaussian process. There is slight degradation in the CDF performance by increasing Δf from 1/50 to 1/10.

Fig. 13 shows the evaluated iteration time (time required to compute each output sample) for the pure MCM and DMCM. This data was obtained by averaging results over 10^5 output samples. The implemented code was written and compiled using the C programming language and all computing times are based on a 1.8GHz Pentium IV processor running Windows XP. As only integer operations are involved in equation (15), the DMCM is seen to have a speed improvement over the pure MCM. The improvement factor is around 2.8, which is independent of the sinusoid number N, the table size N_{Table}, and Δf. With the sinusoid number N set to be less than 800, the DMCM can generate more than 20,000 outputs per second, which is sufficient for shadowing fluctuation processes in system level simulations.

In summary, the MCM approach gives the best performance in terms of ASE versus the number of sinusoids used. The ASE level of the proposed DMCM model is bounded by the USM bound when the frequency sampling resolution is low (i.e. Δf is large). The DMCM can achieve the same ASE performance as the MCM when Δf decreases to a certain threshold. The value of this threshold depends on the number of sinusoids N in the model. Introducing symmetry (which is vital for P2P simulations) degrades the DMCM ASE performance significantly, especially when Δf is large. However, a desired ASE level of say $10^{-2.6}$ (corresponding to a mean absolute error of 0.05) can still be achieved by reducing Δf and/or increasing N.

Model Implementation method

As many of the parameters for DMCM are related, and some of them have significant impact on the model performance, the following step-by-step guide are given on the model implementation for the joint shadowing process in mesh P2P networks in urban environments

Step 1. Determine the parameters of the simulated radio environment, which include:

- The dimension of the virtual shadowing fluctuation map: x_{MAX} and y_{MAX} (i.e. the extent of simulated region)
- The shadowing fluctuation parameters: Standard deviation σ_s and de-correlation distance d_{cor}.

Step 2. Determine the parameters of DMCM, which include:

- the number of sinusoids N: N should be great enough to ensure the model accuracy. It should be noted that the model accuracy is also a function of Δf. According to the performance analyses in previous subsection, for $\Delta f = d_{cor}/20$, N=500 is suggested.
- the frequency resolution Δf: this parameter defines the shadowing process periodicity. Therefore, $1/\Delta f$ must be no less than $\max[x_{MAX}, y_{MAX}]$. For increasing model accuracy, Δf should be as small as possible. However, decreasing Δf increases the size of sinusoidal waveform table N_{Table}, i.e. requires more computer memory, especially when the spatial resolution Δx is set to a very small value. Decreasing Δf also results in larger periodicity, which is undesirable if a user want to wrap a small virtual shadowing map to simulate large networks with a lot of radio nodes (in order to reduce the network simulation time). $\Delta f < 1 / (20\, d_{cor})$ is suggested.
- the spatial resolution Δx: the DMCM model is only able to directly generate the shadowing fluctuations on spatial grids with resolution Δx. For any Tx/Rx location off those grid points, the shadowing fluctuation value has to be spatially interpolated from the values at nearby grid points. The simplest (also the fastest) interpolating method is approximating the shadowing fluctuation by returning the value for the nearest grid point, in which case, Δx must be much less than the distance up to which the mean received power (and hence the shadowing fluctuation value) remains approximately constant. An accepted empirical bound is terminal movement over a few tens of wavelengths [8].
- the table size of stored sinusoidal waveform is calculated by $N_{Table} = 1 / (\Delta x \cdot \Delta f)$

The suggestions on the parameters setting are summarized in Table I.

Step 3. Generate the random 4-D spatial continuous frequency set $\{\mathbf{f}_n\}$ and the phase set $\{\theta_n\}$ using equations (13) and (14) respectively. For the symmetric DMCM, only the first half of each set needs to be generated, with the second half calculated using equations (17) and (19). The coefficients c_n are set to be $\sqrt{2/N}$ for all sinusoids, in order to generate a unity power Gaussian random process (i.e., $\sum c_n^2/2=1$).

Step 4. Transform the continuous frequency set $\{\mathbf{f}_n\}$ and the phase set $\{\theta_n\}$ into discrete forms using equations (15) and (16) respectively.

Having completed the above 4 steps, the virtual shadowing fluctuation map can then be determined. To generate a different shadowing fluctuation map for the same radio scenario, steps 3 and 4 can be repeated. The shadowing fluctuation value between any pair of radio nodes on the virtual map can be calculated using step 5:

Step 5. Calculate the unity power Gaussian value by inputting the Tx and Rx locations (after transformed into discrete forms using Δx) into equation (17). This value is then multiplied by the shadowing fluctuation standard deviation σ_s to obtain the exact shadowing fluctuation.

The physical location of each node can be set manually, or can be randomly generated using a mobility model [34]. It is worth emphasizing that the DMCM method generates a periodic map, and the radio nodes can be considered to lie on the surface of a ring toroid.

VI. Conclusions

In this submission, the spatial correlation of the shadowing fluctuation for P2P radio links has been investigated, and its correlation functions extracted. Statistical analysis revealed that the shadowing fluctuation process is mainly a result of MS movement. Its ACF in single mobility scenario can be well modelled by an exponential

decay function, with the de-correlation distance 20m (for city of Bristol). Furthermore, the joint correlation property of a P2P link in dual mobility scenario showed that MS movement at each end of the link has an independent and equal effect on the correlation coefficient. The JCF can be approximated by the product of two ACF in single mobility scenario.

A novel simulation model for the joint shadowing processes in urban P2P radio channels was proposed. The underlying principle is that a Gaussian random process with a given PSD can be modelled as a sum of sinusoids. The spatial frequencies of the sinusoidal waveforms were determined using a Discrete Monte Carlo Method. It generates periodical output, which wraps the simulated radio environment, and enables users to simulate large networks without fear of interference edge effect. In addition, this method can also be efficiently implemented on a computer (or hardware platform) by using look-up table techniques, which improves the simulation speed. Simulations illustrated that the proposed model is capable of generating shadowing fluctuation output values that approximate the Gaussian distribution (in dB) and with the desired correlation property, and improves accuracy or speed performances compared to other considered methods. In conclusion, the proposed model enables extensive system level simulations of large P2P urban radio networks with correlated shadowing.

TABLE I
PARAMETERS SETTING GUIDE LINE

Parameters	Symbol	Suggested Value
Shadowing Standard deviation	σ_s	8 -12 dB [33] or Advanced P2P link shadowing model [23]
Shadowing de-correlation distance	d_{cor}	20m for typical European city
Number of sinusoids	N	N = 500
Frequency resolution	Δf	$\Delta f < 1 / (20\ d_{cor})$, and the map periodicity $1/\Delta f > MAX(x_{MAX}, y_{MAX})$
Spatial resolution	Δx	Δx < 10 wavelengths
Waveform table size	N_{Table}	$N_{Table} = 1 / (\Delta x \cdot \Delta f)$

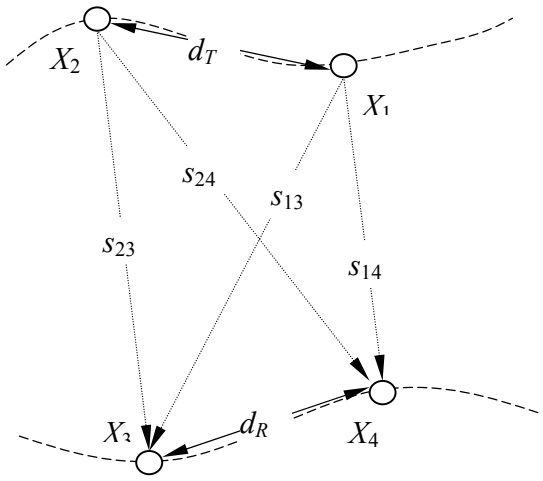

Fig. 1. Ad-hoc System model

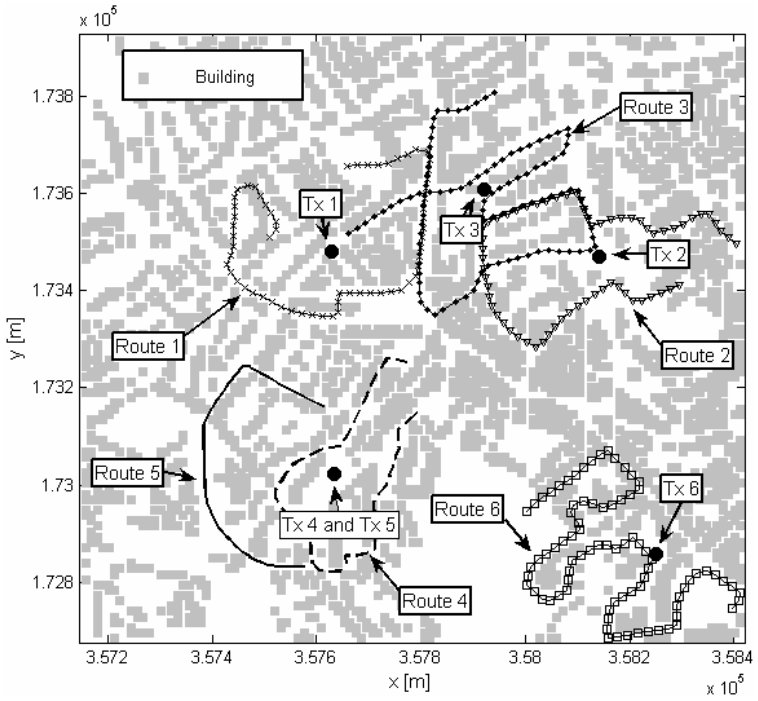

Fig. 2. Route settings for single terminal mobility scenario

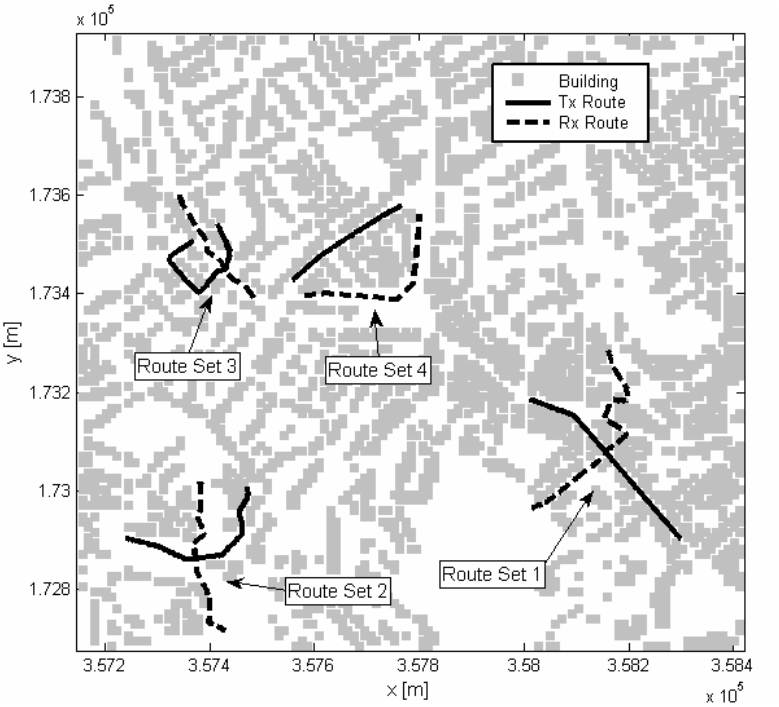

Fig. 3. Route settings for dual terminal mobility scenario

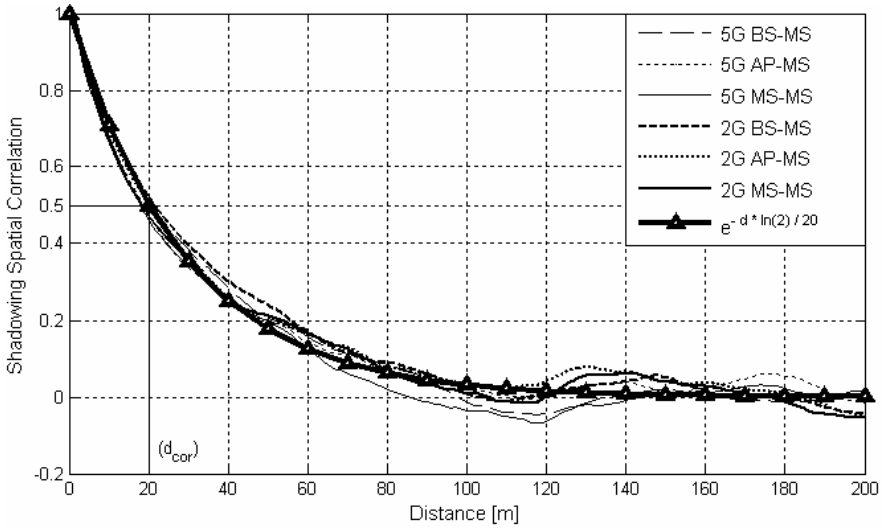

Fig. 4. ACF from single terminal mobility scenario simulations

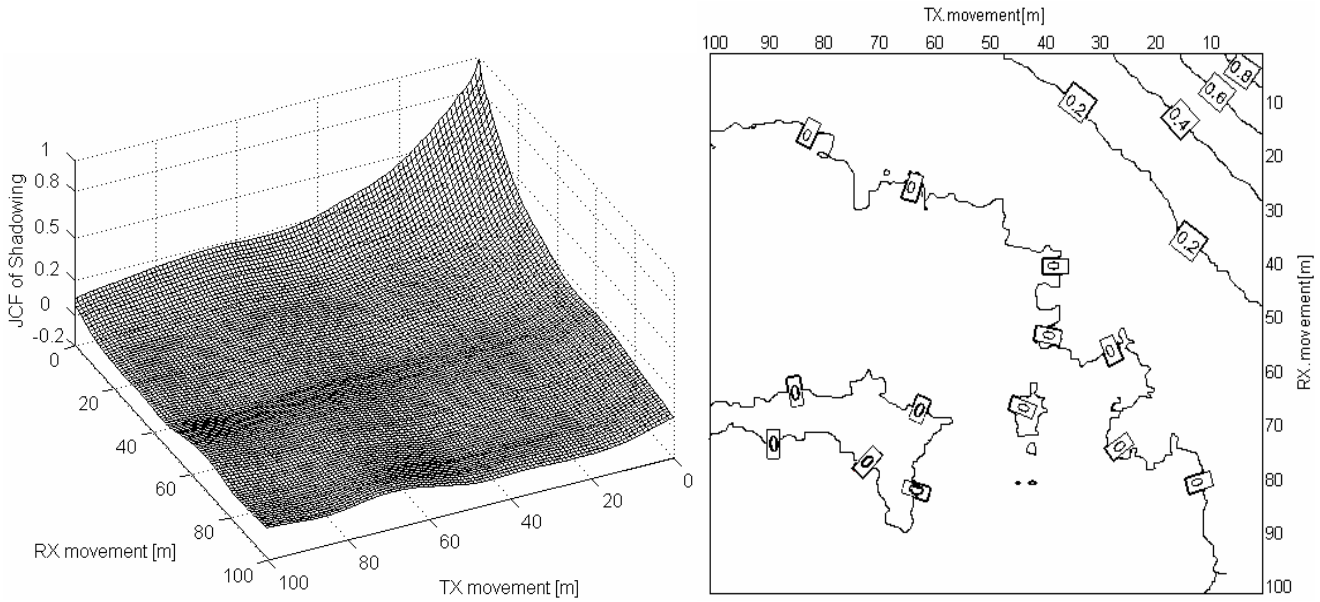

(a) (b)

Fig. 5. JCF from dual terminal mobility scenario simulations, (a) 3D plot, and (b) contour plot

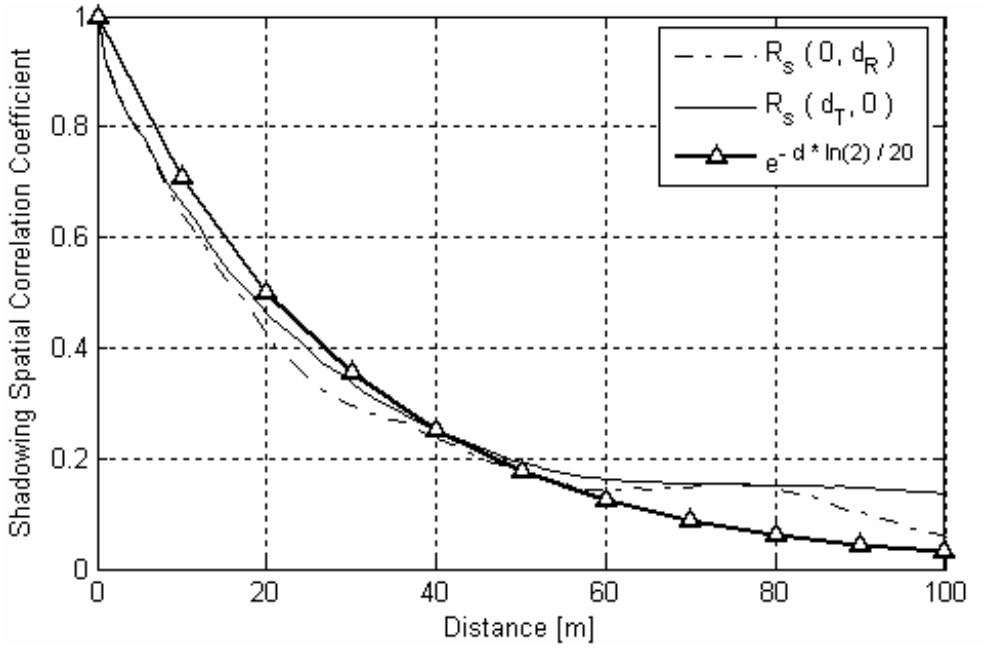

Fig. 6. Comparison between ACF and sliced sections of the JCF

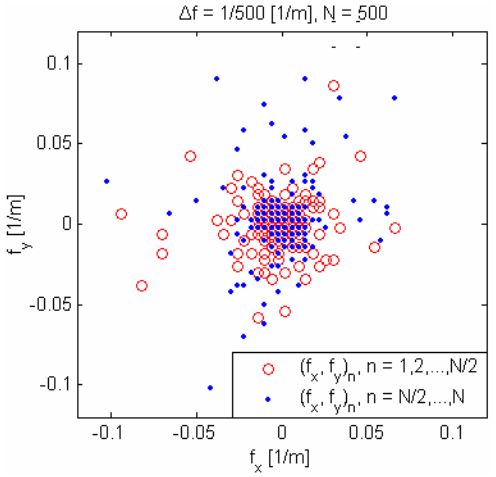

Sample frequencies

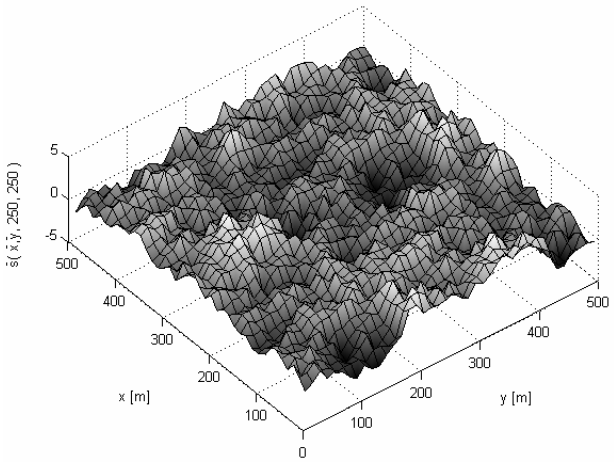

Sample of Shadowing process

Fig. 7. A realization of the DMCM method

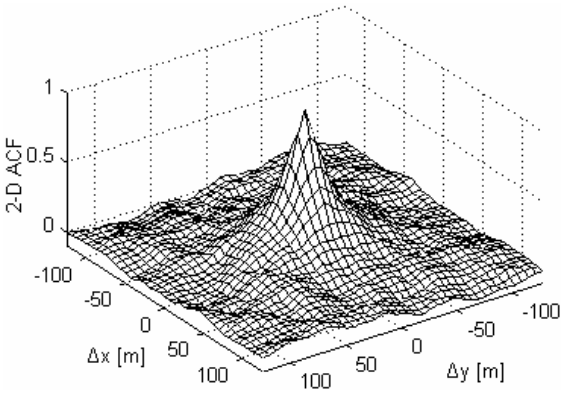

(a) Evaluated 2D ACF

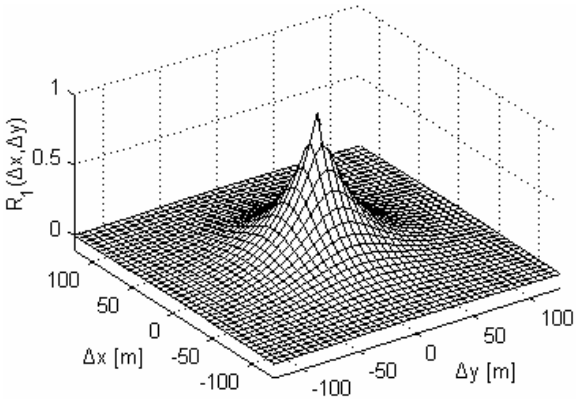

(b) Theoretical 2D ACF

Fig. 8. Comparison of the evaluated and theoretical 2D ACF

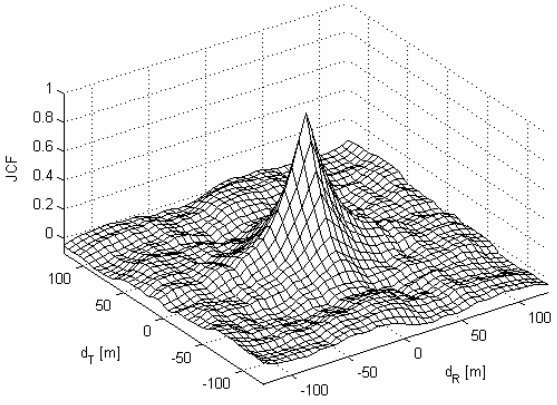

(a) Evaluated JCF

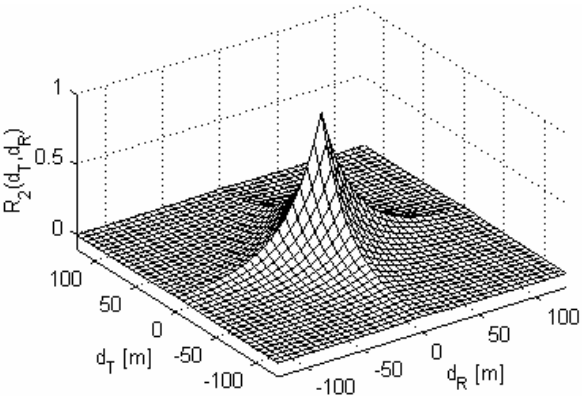

(b) Theoretical JCF

Fig. 9. Comparison of the evaluated and theoretical JCF

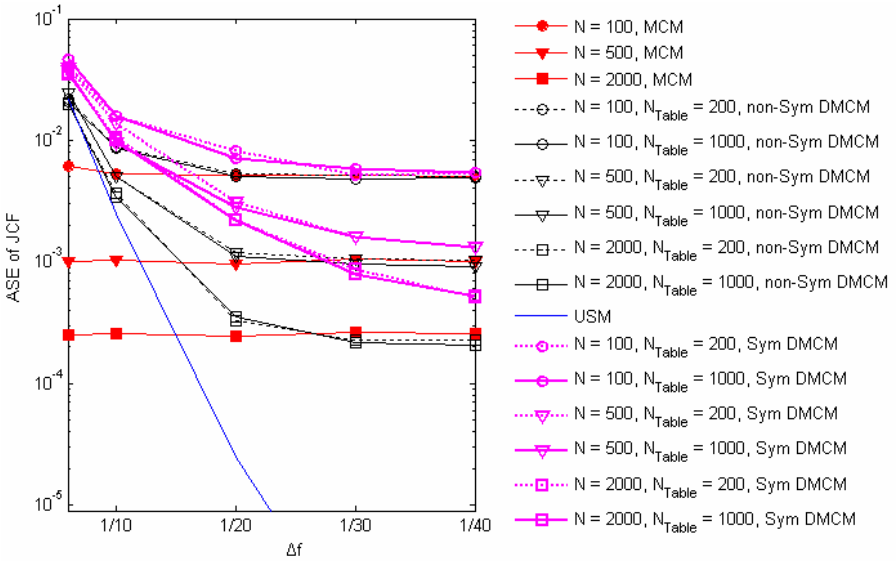

Fig. 10. ASE level JCF

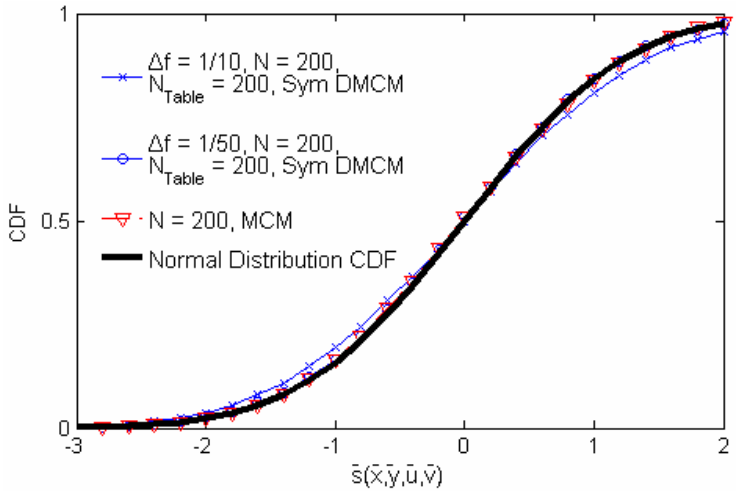

Fig. 12. CDF of the output value

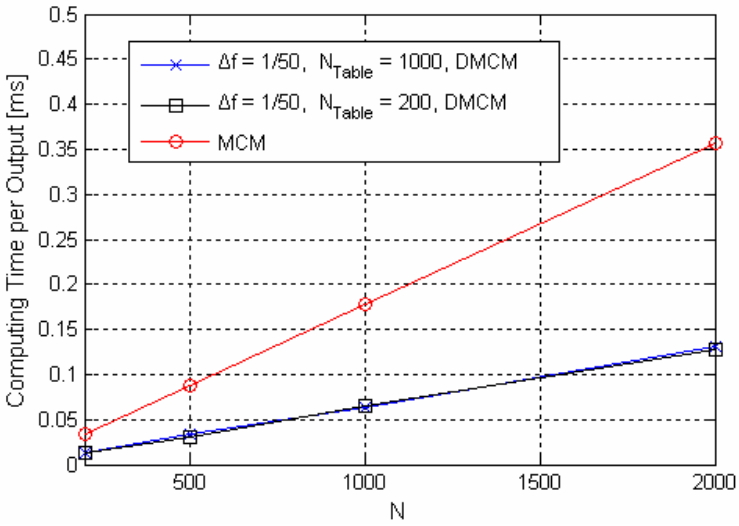

Fig. 13. Simulation speed comparison

References

[1] R. Ramanathan and J. Redi, "*A Brief Overview of Ad Hoc Networks: Challenges and Directions*" IEEE Comm. Magazine, May 2002.

[2] A. Doufexi, et al, "*A comparison of the HIPERLAN/2 and IEEE802.11a wireless LAN standards,*" IEEE Commun. Mag., vol. 40, pp. 172–180, May 2002.

[3] 3GPP TR 25.924 V1.0.0. 3GPP TSG-RAN, "*Opportunity Driven Multiple Access*", Dec. 1999.

[4] J. Vidal, et al. "*Multihop networks for capacity and coverage enhancement in TDD/UTRAN*", MedHocNet 2002, Sardinia (Italy), September 2002.

[5] A. N. Zadeh et al, *"Self-Organising Packet Radio Ad hoc Networks with Overlay (SOPRANO)",* IEEE Communications Magazine, June, 2002.

[6] M. Lott et al, "*Medium Access and Radio Resource Management for Ad Hoc Networks based on UTRATDD*", MobileHOC, 2001.

[7] "*Digital Mobile Radio Towards Future Generation Systems*", COST 231 Final Report, Chapters 2, 4, 1998.

[8] L. M. Correia, "*Wireless flexible personalized communications, COST 259: European co-operation in mobile radio research*" ISBN 0471 49836X, pp.77-222, 2001.

[9] M. Gudmundson, *"Correlation model for shadow fading in mobile radio systems,"* Electron. Lett. vol. 27, pp. 2145–2146, Nov. 1991.

[10] A. Gehring, M. Steinbauer, I. Gaspard, and M. Grigat, *"Empirical channel stationarity in urban environments",* EPMCC, Feb. 2001.

[11] X. Cai and G. Giannak, *"A Two-Dimensional Channel Simulation Model for Shadowing Processes"*, IEEE Trans. Veh. Technol., vol. 52, Nov. 2003.

[12] H. Kim and Y. Han, "*Enhanced Correlated Shadowing Generation in Channel Simulation*", IEEE Commun. Letters, vol. 6, no, 7, July 2002.

[13] F. Graziosi and F. Santucci, *"A General Correlation Model for Shadow Fading in Mobile Radio Systems",* IEEE Commun. Letters, vol. 6, no. 3, Mar 2002

[14] N. Patwari, Y. Wang and R. J. O'Dea, "*The importance of the multipoint-to-multipoint indoor radio channel in ad hoc networks,*" in IEEE Wireless Commun. and Networking Conf., (Orlando, FL), pp. 608-612, Mar. 2002

[15] ftp://ftp.3gpp2.org/TSGC/Working/2003/3GPP_3GPP2_SCM, *Spatial Channel Model Text Description v7.0*, 3GPP2, August 19, 2003

[16] E K Tameh and A.R. Nix, "*A 3-D integrated macro and microcellular propagation model, based on the use of photogrametric terrain and building data"*, IEEE VTC'97 Proceedings, Phoenix, May 1997

[17] E. K. Tameh and A.R Nix, "*A Mixed-Cell Propagation Model for Interference Prediction in a UMTS Network"*, IEEE VTC 2001 Proceedings, Rhodes, May 2001.

[18] S. O. Rice, "*Mathematical analysis of random noise*," Bell Syst. Tech. J., vol. 23, pp. 282–332, July 1944.

[19] M. Pätzold, U.Killat and F. Laue, "*A deterministic digital simulation model for Suzuki processes with application to a shadowed Rayleigh land mobile radio channel*," IEEE Trans. Veh. Technol., vol. 45,

May 1996.

[20] M. Pätzold and V. D. Nguyen, "*A Spatial Simulation Model For Shadow Fading Processes In Mobile Radio Channels,*" PIMRC 2004, Barcelona, Spain, September 2004

[21] M. Patzöld, U. Killat, F. Laue and Y. Li, "*On the statistical properties of deterministic simulation models for mobile fading channels,*" IEEE Trans. Veh. Technol., vol. 47, Feb. 1998.

[22] M. Patzöld, R. Farcía and F. Laue, "*Design of high-speed simulation models for mobile fading channels by using table look-up techniques*," IEEE Trans. Veh. Technol., vol. 49, July 2000.

[23] Z Wang, E. K. Tameh and A. R. Nix, *"Statistical Peer-to-Peer Channel Models for Outdoor Urban Environment at 2GHz and 5GHz"*, IEEE VTC Fall 2004, Los Angeles, 2004.

[24] B. Sklar, "*Rayleigh Fading Channels in Mobile Digital Communication Systems Part 1: Characterization,*" IEEE Comm. Magazine, July 1997.

[25] W. C. Y. Lee, "*Mobile Communications Engineering*". 1997, McGraw-Hill, ISBN 0070371032, 1997.

[26] W. C. Jakes, *Microwave Mobile Communications*. Piscataway, NJ: IEEE Press, 1994.

[27] E. Lutz and E. Plöchinger, "*Generating Rice processes with given spectral properties*," IEEE Trans. Veh. Technol., vol. VT-34, pp. 178–181, Nov. 1985.

[28] S. A. Fechtel, "*A novel approach to modeling and efficient simulation of frequency-selective fading radio channels*," IEEE JSAC., vol. 11, pp. 422–431, Apr. 1993.

[29] A. Papoulis and S. Pillai, *Probability, Random Variables and Stochastic Processes*. McGraw-Hill, 4th ed, 1973.

[30] H. S. Wang and N. Moayeri, "*Finite-state Markov channel - A useful model for radio communication channels*," IEEE Trans. Veh. Technol., vol. 44, pp. 163–171, Feb. 1995.

[31] C. Iskander and P. T. Mathiopoulos, "*Fast Simulation of Diversity Nakagami Fading Channels Using Finite-State Markov Models*", IEEE Trans. on Broadcasting, vol. 49, no. 3, Sept. 2003.

[32] P. Höeher, "*A statistical discrete-time model for the WSSUS multipath channel*," IEEE Trans. Veh. Technol., vol. 41, pp. 461–468, Nov. 1992.

[33] L. M. Correia, "Wireless flexible personalized communications, COST 259: European co-operation in mobile radio research" ISBN 0471 49836X, pp.77-222, 2001.

[34] T. Camp, J. Boleng, V. Davies, "*A survey of mobility models for ad hoc network research. Wireless Communications & Mobile Computing*", (WCMC): Special Issue on Mobile Ad Hoc Networking: Research, Trends, and Applications, vol. 2, no. 5, 483–502. 2002